

## The E760 lead-glass central calorimeter: design and initial test results \*

L. Bartoszek, V. Bharadwaj, M.D. Church, A.A. Hahn, J. Peoples Jr., S.H. Pordes, P.A. Rapidis and S.J. Werkema

*Fermi National Accelerator Laboratory, P.O. Box 500, Batavia, IL 60510, USA*

D. Agahi \*\*, D.R. Broemmelsiek, J.E. Fast, M. Gee, K.E. Gollwitzer, M.A. Mandelkern, J.L. Marques, J. Schultz and M.F. Weber

*Department of Physics, University of California, Irvine, CA 92717, USA*

C.M. Ginsburg, M. Masuzawa, R.E. Ray, J.L. Rosen, S. Trokenheim and J.L. Zhao

*Department of Physics, Northwestern University, Evanston, IL 60201, USA*

T.A. Armstrong, G.E. Hufford \*\*, R.A. Lewis, A.M. Majewska, J.D. Reid and G.A. Smith

*Laboratory for Elementary Particle Science, Department of Physics, Pennsylvania State University, University Park, PA 16802, USA*

M.A. Hasan +

*Department of Physics, Pennsylvania State University, York, PA 17403, USA*

C. Biino and S. Palestini

*Istituto Nazionale di Fisica Nucleare, sez. Torino, Via P. Giuria 1, 10125 Torino, Italy*

Received 20 September 1990

The central calorimeter in Fermilab experiment E760 ++ has been designed to measure the topology and energies of electrons and photons in the decay of charmonium formed in  $p\bar{p}$  annihilation. The calorimeter is composed of 1280 lead-glass Cherenkov counters read out with photomultiplier tubes. This paper discusses design criteria for the calorimeter and describes how these criteria were met. Data from tests in low energy (10–84 MeV) and medium energy (1–4 GeV) beams are presented showing a spatial resolution of 9 mm, an energy resolution of  $(3.0 \pm 0.3)\% / \sqrt{E[\text{GeV}]} + (1.5 \pm 0.5)\%$ , and an effective energy threshold below 10 MeV.

### 1. Introduction

Charmonium states have been studied extensively in  $e^+e^-$  collider machines [1]. Their direct formation in these machines is restricted to states that have the quantum numbers of the photon state ( $J^{PC} = 1^{--}$ ),  $J/\psi$ ,  $\psi'$ , etc. Other charmonium states (e.g.,  $\chi$ 's,  $\eta_c$ 's)

have been observed by the photon emission to/from the  $J/\psi$  and  $\psi'$ . The measurement of masses and widths of these states is limited by the resolution of the photon energy measurement, which is typically 10–25 MeV [2].

Charmonium can also be produced through resonant  $p\bar{p}$  annihilation; this process is not restricted to producing states with  $J^{PC} = 1^{--}$ . Among the many charmonium states that can be formed in this manner, there are several predicted narrow states, including the  $^1P_1(1^{+-})$ ,  $^1D_2(2^{-+})$ , and  $^3D_2(2^{--})$  states which have not yet been confirmed [3]. Experiment E760 has been designed to measure the masses and widths of these charmonium states with high precision, using  $p\bar{p}$  annihilation in an internal hydrogen gas jet target [4] installed in the AP50 straight section in the Antiproton Accumulator at

\* Work supported in part by the U.S. National Science Foundation and the U.S. Department of Energy.

\*\* U.S. National Science Foundation Research Experiences for Undergraduates (REU) Awardee.

+ Work supported in part by a Research Opportunity Award from the U.S. National Science Foundation.

++ Fermilab–Ferrara–Genova–U.C. Irvine–Northwestern–Penn. State–Torino collaboration.

Fermilab [5]. The mass resolution is given by the beam momentum spread and in the mass range 2.9–3.9 GeV/ $c^2$  is approximately 300 keV/ $c^2$  rms. The feasibility of such an experiment was first shown at the CERN ISR in experiment R704 [6].

The E760 detector layout is shown in fig. 1. The detector has been designed to detect electromagnetic decays of charmonium states efficiently, while at the same time rejecting large (typically  $10^7$  times larger) nonresonant hadronic background. It consists of scintillation hodoscopes and vetos, tracking chambers [7], a segmented Cherenkov counter, a luminosity monitor, a forward end-cap sampling electromagnetic calorimeter [8], and a central lead-glass electromagnetic calorimeter, which is the subject of this article.

Section 2 describes the design of the calorimeter and the choices made for materials and photomultipliers. Section 3 presents the construction and initial calibration of the system. Section 4 describes test made at the University of Illinois Nuclear Physics Laboratory (UINPL) with electrons and photons below 100 MeV. Section 5 discusses studies of a section of the calorimeter in a Brookhaven National Laboratory (BNL) test beam with electrons and pions from 1 to 4 GeV and the determination of the energy and position resolutions of the device. Section 6 presents preliminary results for the  $J/\psi \rightarrow e^+e^-$  at Fermilab and section 7 states conclusions.

## 2. Design considerations

In experiment E760 the central calorimeter serves to detect electrons and  $\gamma$ 's from charmonium decays for final state identification and reconstruction. The formation mass of the state is given by the energy of the circulating antiproton beam as determined from the revolution frequency and the orbit length, and not from the event reconstruction of the final state. Thus the

experiment requires a large acceptance electromagnetic calorimeter capable of distinguishing signal from background events, both at the trigger level and offline. The backgrounds are most severe in neutral final states containing  $2\gamma$  and  $3\gamma$  and are due to the reaction  $p\bar{p} \rightarrow 2\pi^0$ . The  $2\pi^0$  final state can mimic a  $2\gamma$  or  $3\gamma$  final state when one or both  $\pi^0$ 's decay asymmetrically and the low energy  $\gamma$  is not detected. To control this background,  $\gamma$ 's with energy above 50 MeV have to be detected with an efficiency of 95%. In addition, a  $\pi^0$  which decays symmetrically can appear as a single  $\gamma$  if the showers from the two decay  $\gamma$ 's are not resolved. The granularity of the calorimeter had to be sufficient to recognize such decays.

### 2.1. Calorimeter material

Of the materials considered (CsI, NaI, BaF<sub>2</sub>, BGO, lead-scintillator fibers, and lead glass), lead glass was chosen on the basis of cost, handling, and ease of manufacture. The particular type of lead glass was selected to maximize light output. Comparative studies of five lead glasses were performed with low energy  $\gamma$ 's at UINPL (see section 4). It was found that F2 lead glass (see table 1) gives twice as much light as SF5 glass due to the longer path length of shower electrons and the superior light transmission. It was chosen despite its longer radiation length (3.13 cm vs 2.54 cm) and somewhat poor radiation damage properties. In particular, it was found that the radiation dose (<sup>137</sup>Cs  $\gamma$ 's) which reduces the transmission of 400 nm light through a 40 cm F2 block by a factor 2 is about 300 rad, compared to about 400 rad for a 40 cm SF5 block, in agreement with previous measurements [9].

### 2.2. Geometry

The calorimeter is cylindrical and covers 360° in azimuth, and 10° to 70° in polar angle, and represents

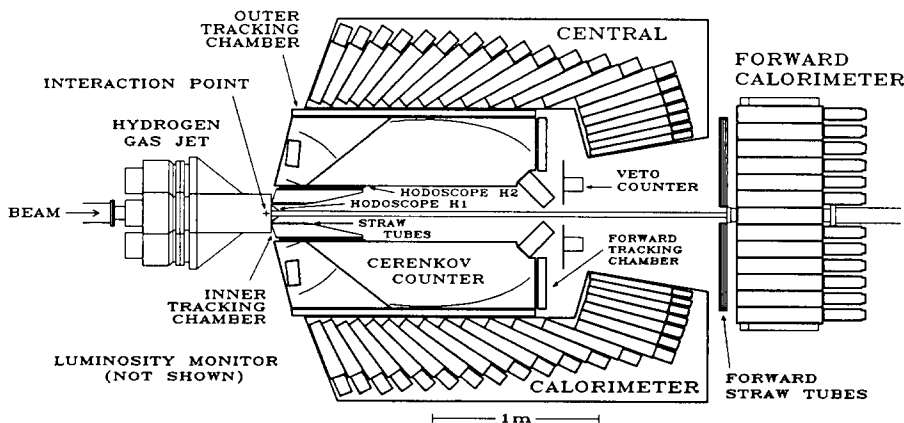


Fig. 1. E760 detector layout at the Antiproton Accumulator at Fermilab.

Table 1  
Characteristics of lead-glass type F2

Manufacturer:	
Schott Glass Technologies, Inc.	
Duryea, PA, USA	
Composition by weight:	
Lead	42.2%
Silicon	21.4%
Oxygen	29.5%
Potassium	4.2%
Sodium	2.3%
Arsenic	0.15%
Density	3.61 g/cm <sup>3</sup>
Radiation length ( $L_R$ )	3.141 cm
Refractive index (at 404.7 nm)	1.651
Transmission properties:	
Wavelength [nm]	Transmittance (10 cm)
335–344	56.9%
385–394	95.5%
435–444	97.9%
485–494	98.4%
535–544	98.9%
585–594	99.4%

an approximate 70% acceptance for charmonium decays of interest. Angles below  $10^\circ$  are covered by the forward electromagnetic calorimeter, and the equipment of the internal hydrogen gas jet target prevents coverage beyond  $70^\circ$ . The calorimeter consists of lead-glass blocks, each coupled to a photomultiplier. The blocks are tightly packed together, separated by thin septa of stainless steel. A pointing geometry for the blocks was chosen to allow a simple analysis of event topology,

especially online in a high rate ( $10^6$  interactions/s) environment.

A Monte Carlo simulation was made to determine the required calorimeter granularity. The granularity was chosen so that symmetrical  $\pi^0$  decay at the highest formation energy contemplated for the experiment produces two resolvable clusters in the lead glass. This consideration leads to a 64-fold segmentation in the azimuthal angle  $\phi$  and a 20-fold segmentation in the polar angle  $\theta$ . The glass blocks subtend angles varying from  $1.1^\circ$  (at  $\theta = 10^\circ$ ) to  $5.2^\circ$  (at  $\theta = 70^\circ$ ) as seen in table 2.

The lengths of the glass blocks were chosen according to a number of considerations. The Monte Carlo studies demonstrated that an optimized energy resolution is not crucial in suppressing background events, while sensitivity to low energy  $\gamma$ 's is. Consequently block lengths were chosen to confine 90–95% of shower energies, leading to lengths varying from 12 radiation lengths ( $L_R$ ) at  $70^\circ$  to  $16L_R$  at  $10.6^\circ$  (table 2). Such short blocks have improved sensitivity to low energy  $\gamma$ 's due to reduced light transmission losses.

### 3. Calorimeter construction

The calorimeter is divided into 64 equal sections in  $\phi$  (fig. 2), each section called a wedge. Within each wedge there are 20 blocks of lead glass [10], arranged to provide a pointing geometry to the target, with each block covering the same interval in pseudorapidity. This gives the blocks the shape of an erect pyramidal frustum with a regular trapezoidal base.

#### 3.1. Counter

The lead-glass blocks were polished to a plate glass polish [11] and the edges had a 2 mm chamfer of

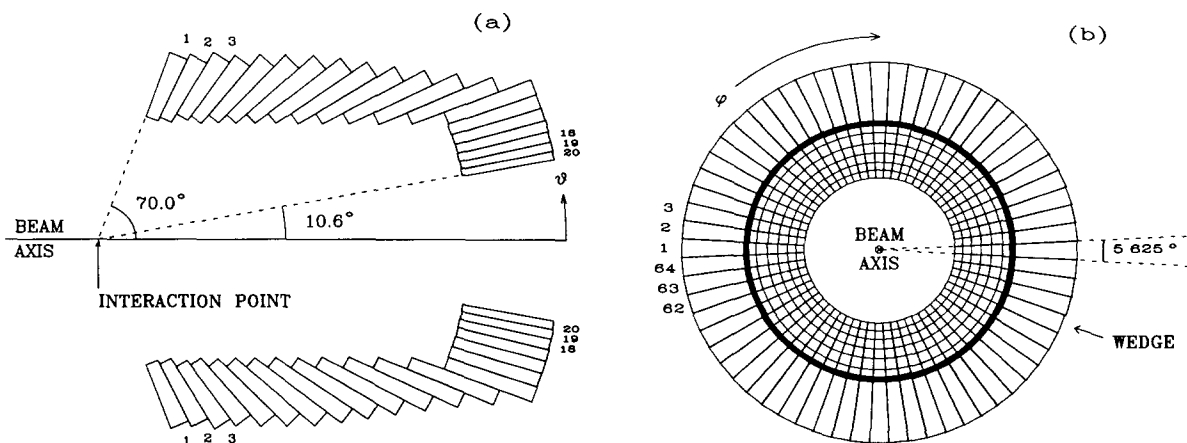


Fig. 2. Two views of calorimeter: (a) side view showing the  $\theta$  coverage and numbering of blocks in a wedge and (b) end view of the 64 wedges along the beam axis.

Table 2  
Dimensions and positions of lead-glass blocks in a wedge

Block number	Length [ $L_R$ units]	$\Delta\theta$ [deg]	$\Delta\phi$ [deg]	Distance from target <sup>a</sup> [cm]	Fractional PMT coverage
1	12.03	5.226	5.625	72.44	0.473
2	12.30	5.031	5.625	75.87	0.475
3	12.70	4.803	5.625	80.07	0.476
4	13.21	4.552	5.625	85.08	0.478
5	13.86	4.284	5.625	90.96	0.479
6	14.65	4.007	5.625	97.79	0.481
7	15.59	3.728	5.625	105.62	0.482
8	15.92	3.451	5.625	114.54	0.497
9	15.92	3.183	5.625	124.66	0.520
10	15.92	2.925	5.625	136.07	0.544
11	15.92	2.679	5.625	148.89	0.568
12	15.92	2.449	5.625	163.26	0.593
13	15.92	2.233	5.625	179.34	0.617
14	15.92	2.033	5.625	197.28	0.641
15	15.92	1.848	5.625	197.29	0.546
16	15.92	1.678	5.625	197.29	0.664
17	15.92	1.522	5.625	197.30	0.527
18	15.92	1.380	5.625	197.30	0.644
19	15.92	1.250	5.625	197.30	0.443
20	15.92	1.131	5.625	197.30	0.543

<sup>a</sup> To front face of block.

ground glass finish. A PMT is glued to the back of each block with Epotek 301 epoxy [12] (fig. 3). This epoxy is semiflexible and has an index of refraction of 1.538 and excellent light transmission above 320 nm. A fiber optics

cable is mounted at the back of block. The assembly sequence for each block included a check of size tolerances, a relative transmission measurement with a spectrophotometer, gluing of the PMT and a light-fiber

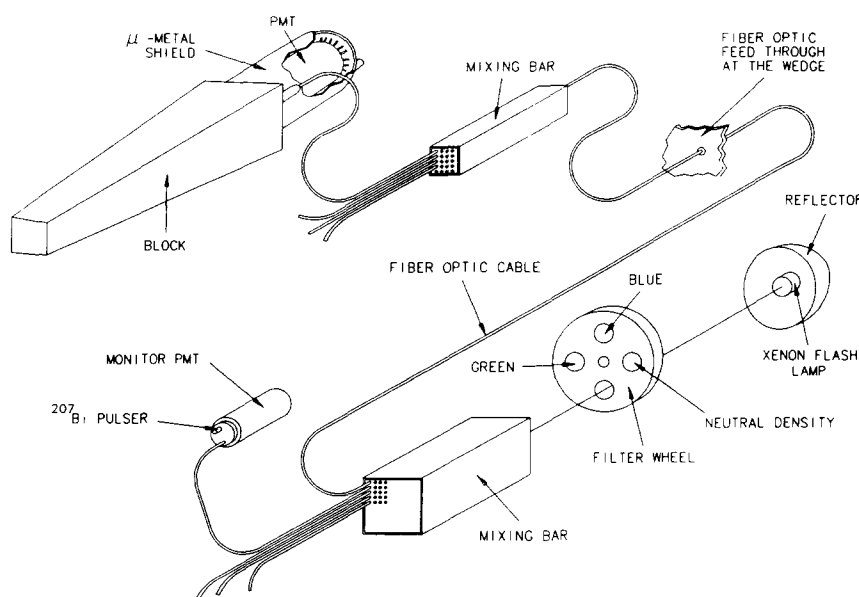


Fig. 3. Sketch of block 7, the mounted PMT and the light path for the xenon flash lamp system.

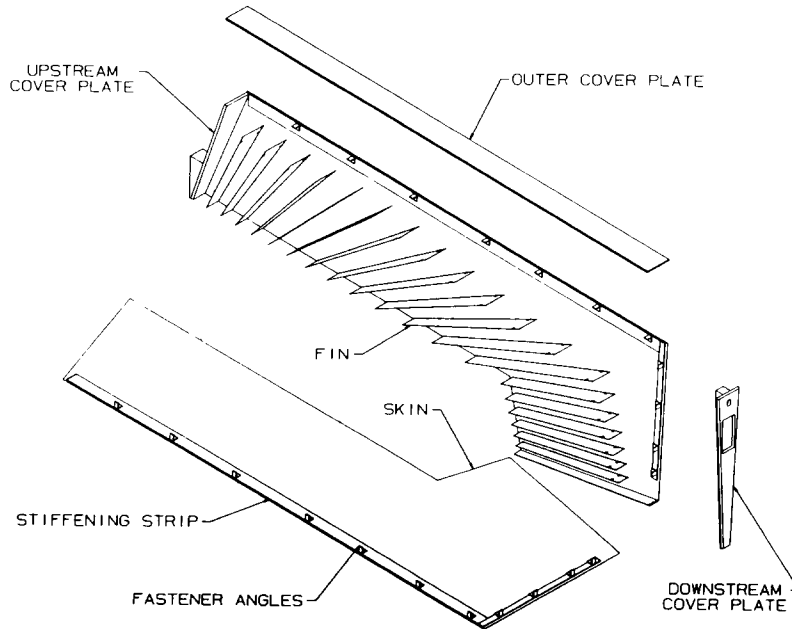


Fig. 4. A cut-out view of a wedge showing the pockets, formed by the shell skins and fins, where the lead-glass blocks are inserted.

connector, wrapping of the  $\mu$ -metal shield [13] around the PMT and a paper wrap of the block. The initial calibration was performed with cosmic rays. The operating voltages were established using results from the BNL tests (section 5).

### 3.2. Wedge and calorimeter assembly

Each wedge is an independent mechanical and electrical unit consisting of the 20 lead-glass counters contained in a light-tight stainless steel shell. The surfaces of the shell (skins; separating the wedges in  $\phi$ ) are 0.735 mm thick, while the thin plates of stainless steel separating the blocks in theta (fins) within the shell are 0.254 mm (fig. 4). The material of the shell covers 2% of the azimuthal and less than 0.5% in  $\theta$ . The shell surfaces and the thin plates were cut and welded together by a laser [14]. Tight tolerances, typically 0.08 mm, were required on both the lead-glass blocks and stainless steel shell to ensure that the counters, when wrapped in a paper cushion, fit properly into the pockets of the shell and that the wedges fit together to form the cylindrical calorimeter. In this configuration the glass serves also as a structural element carrying compressive loads. The tight tolerances of the transverse dimensions of the glass blocks are due to this feature. Significant inter-block gaps would allow the blocks to distort and would introduce tensile stresses due to bending. These gaps were kept at a magnitude that did not allow the tensile stresses to exceed  $1.04 \times 10^7$  Pa.

Assembly of a wedge consisted of insertion of 20

lead-glass blocks into the pockets of the shell, attachment of a mechanical support to the thin plates between the blocks in the wedge to seat and hold the blocks in place, installation of fiber optic and electrical cable harnesses and installation of covering panels. All of the cables are fed through the downstream panel using block connectors [15] and a fiber optic feedthrough. The inner panel is made of opaque PVC. The downstream

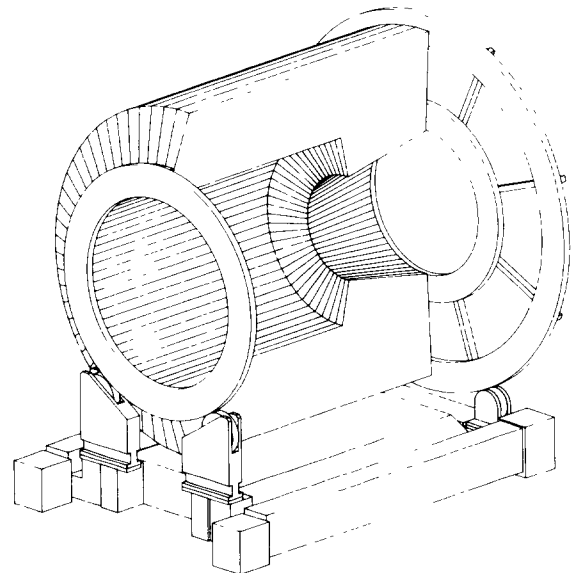


Fig. 5. Isometric view of the calorimeter and its support structure.

Table 3  
Characteristics of photomultiplier tubes

Manufacturer	Hamamatsu Corporation, Hamamatsu City, Japan				
Photocathode material	Bialkali				
Window material	Borosilicate glass				
Dynode structure	Linear focused				
Sensitivity range	300–650 nm				
Peak sensitivity	420 nm				
Dimensions, variability in photocathode efficiency, and gain equation parameter $m$ :					
Model number	Diameter [in.]	Length [in.]	Photocathode efficiency [rms/mean]	$m$ [rms/mean]	Number of dynodes
R3036-02	3.0	5.0	0.10	0.038	12
R3345-02	2.5	5.0	0.14	0.034	12
R2154-04	2.0	6.0	0.13	0.027	10
R580-13	1.5	6.0	0.13	0.026	10

and outer panels are made of black anodized aluminum to reduce stray reflections of light and thus minimize cross-talk.

Each fully assembled wedge weighs approximately 275 kg. Three massive rings are used to support the wedges. They rest on rollers that allow the calorimeter to rotate in  $\phi$  facilitating the replacement of a wedge. The calorimeter and its support structure are shown in fig. 5. The overall support structure was designed to be sufficiently rigid so that no additional stresses are induced on the glass during movement or transport of the calorimeter. The calorimeter with its support structure weighs 23 t. It is mounted on five air casters which allow it to be moved and positioned onto the beam line. Precision alignment to the beam is accomplished by four motorized screw jacks and eight hydraulic cylinders. The entire calorimeter can be aligned to an accuracy of  $\pm 0.0051$  cm.

### 3.3. Photomultipliers

Photomultiplier tubes (PMT) were chosen to maximize light collection, to provide a linear dynamic range suitable to the several MeV to several GeV shower range of the experiment, and with gains capable of driving FERA ADCs [16]. It is desirable that the PMTs be insensitive to magnetic fields of up to 1.5 G, since it was difficult to place  $\mu$ -metal shields extending forward of the photocathode. To maximize light collection photomultipliers of four diameters were used; 3 in. (896 pieces), 2.5, 2, and 1.5 in. (128 pieces each) (see table 3). Linear focused PMTs, 3 in. in diameter, from three manufacturers were evaluated. It was found that the PMTs with good timing precision are inferior in light

collection. Two PMTs specifically manufactured for this experiment, EMI D640 and Hamamatsu R3036, have relatively long rise times (6–10 ns) but excellent light collection. The latter was selected for the experiment on the basis of price. Hamamatsu furnished a 2.5 in. PMT with the same internal structure. The 2 and 1.5 in. PMTs were catalog items. Magnetic field susceptibility was studied for the PMTs under consideration. For the Hamamatsu R3036 (3 in.) and R3345 (2.5 in.) PMTs the pulse height loss due to a 1 G axial (transverse) field was measured to be 5% (14%). The Hamamatsu R580 (2 in.) is somewhat more sensitive to transverse fields and the Hamamatsu R1398 (1.5 in.) is essentially immune to magnetic fields below 2 G.

For all photomultipliers used the relative photocathode efficiencies and gains were measured. This was accomplished by exposing the PMTs to a pulsed LED for which variation in the PMT output pulse height is determined by photoelectron (pe) statistics. The variability (rms/mean) of the parameter  $m$  defined as the exponent of the voltage in the PMT gain equation ( $\text{gain} = \text{const.} \times V^m$ ) and the photocathode efficiencies are listed in table 3. By comparing the pulse heights due to the LED tests and electron induced showers in sample counters, photoelectron yields per MeV were found for all of the counters built. In order to verify the linearity of the photomultipliers the response to a 355 nm pulsed laser was studied. It was found that the greatest deviations from linearity for a range up to 1000 pc output were 8, 5, 5 and 6% for the four PMT types, respectively. The photomultipliers operate at positive high voltage with a bleeder current of approximately 200  $\mu$ A. Base circuits were supplied with the photomultipliers as integral assemblies. Fig. 6 shows the 2.5 and 3

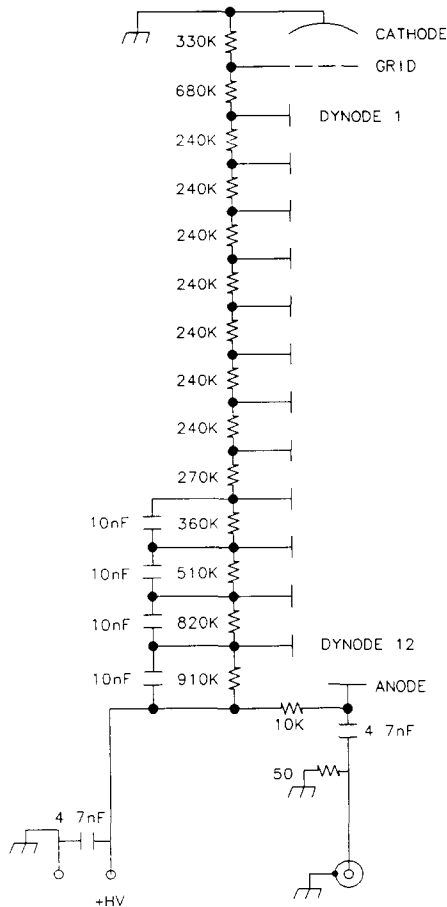


Fig. 6. Base diagram for 2.5 and 3 in. PMTs.

in. PMT base circuit. The gains for each counter are set such that 2000 pc at the anode corresponds to 5 GeV deposited by an electromagnetic shower.

### 3.4. Gain monitoring system

To monitor the counters a system has been developed which uses a single xenon flashlamp [17] as a light source and plastic polymer fiber optic cables [18] to distribute the light to all 1280 channels (see fig. 3). The xenon flashlamp produces a 300 ns pulse whose spectrum has a maximum at 400 nm. The light is collected by an elliptical reflector and is focused into a rectangular lucite mixing bar. A filter wheel allows selection of a neutral spectrum, or blue and green components [19]. The mixing bar uniformly distributes the light into 64 fiber optic cables which are connected one to each wedge [20]. Inside each wedge assembly, the light is further divided by a secondary rectangular mixing bar into 20 fiber optic cables, each of which connects to a lead-glass block [21]. Each counter sees between 1 and 2 GeV energy equivalent of light. Pulse to pulse variation

of the light output as measured by the counters is 12–14%. The total length of the fiber optic cables from the flash lamp to the counter is about 6 m. Radiation exposure of fiber optic segments 1 m long demonstrates a transmission loss of less than 0.25% at a  $^{137}\text{Cs}$  dose of 1500 rad. In order to track the pulse-to-pulse intensity changes of the flashlamp, the system incorporates three Hamamatsu R3036 photomultipliers acting as intensity monitors. To monitor long term drifts each monitor tube is equipped with a  $^{207}\text{Bi}$ /plastic scintillator light pulser [22]. Since the xenon flash light has to traverse the length of the block twice to reach the PMT, it also monitors any degradation of the lead glass due to radiation exposure. By measuring the response of the counter to blue and green light separately, effects of radiation damage in the lead glass can be distinguished from degradation due to other sources of change. The BNL tests (see section 5) were used to calibrate a subset of the counters and to relate the pulse heights of straight-through pions to those for electrons showers. Calibration of individual blocks during assembly was accomplished using cosmic ray muons. The in situ calibration of the calorimeter is established using straight-through charged pions,  $J/\psi \rightarrow e^+e^-$  events and  $\pi^0$ 's.

## 4. Low energy tests at UINPL

A study of the relative light output of five different lead glasses was carried out at the Tagged Photon Facility at UINPL. Gamma rays in the range of 7 to 37 MeV were incident upon the central  $1 \times 1 \text{ cm}^2$  of rectangular lead-glass counters with dimensions  $6 \times 6 \times 41 \text{ cm}^3$ . All of the counters were read out with the same

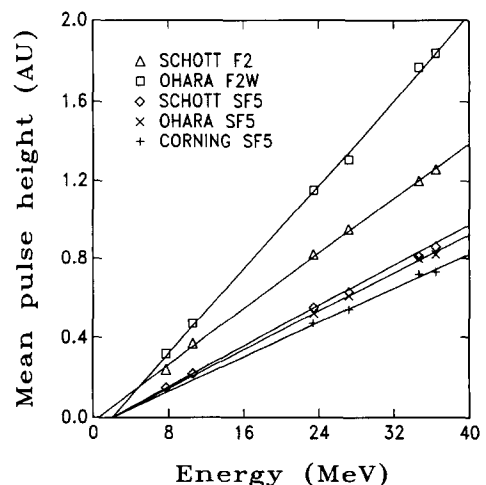


Fig. 7. Mean pulse height distributions for the five lead glasses tested at UINPL. AU indicates arbitrary units.

EMI 9939 photomultiplier, covering 44% of the glass end face and coupled by optical grease. Fig. 7 gives the mean pulse height distribution for the glasses tested. It is noted that within this low energy regime, the light output is linear in photon energy with zero intercept. The F2 glasses are much superior to the SF5 glasses; the Ohara F2W gives twice as much light as any of the SF5 glasses [23]. The Schott F2 piece represents an older manufacturing process and has lower transparency, explaining its relatively poor light output. F2 made currently by all manufacturers, including the glass used in the experiment, is equivalent to the Ohara F2W in transparency. For all of the glasses, 8 MeV  $\gamma$ 's can be clearly observed. In these tests, about 2.5 photoelectrons/MeV were obtained with the F2W blocks using a PMT significantly worse in light collection capability than those used for the calorimeter.

In a subsequent test, five of the final calorimeter counters were exposed to the 88 MeV electron beam. This was done to study the light output per MeV at low energies and to compare it with the performance at high energies as measured at BNL.  $^{207}\text{Bi}$ /plastic scintillator light pulsers were used to maintain the counter calibration. The light output per MeV at 88 MeV was about 90% of the output per MeV measured at BNL between 1 and 4 GeV.

## 5. Tests at BNL

### 5.1. Goals

Three completed wedges, consisting of a total of 60 lead-glass blocks, were tested in the Medium Energy Separated Beam (MESB-B2) at BNL. For these tests a  $^{207}\text{Bi}$  source was glued to the front face of each of the sixty blocks to monitor their gain. The basic goals for the tests were to:

- i) measure energy resolution and linearity with a well defined beam for the different block shapes;
- ii) assess energy loss and sharing, and degrading of energy resolution across boundaries between blocks;
- iii) measure the equivalent energy of straight-through

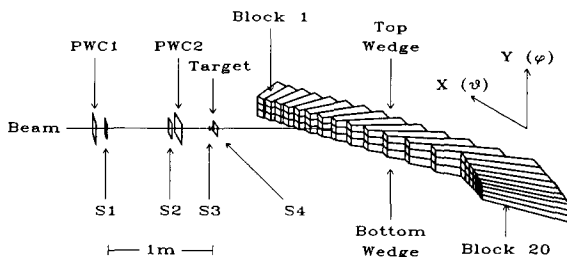


Fig. 8. The three wedge setup in the MESB (B2) beam line at BNL.

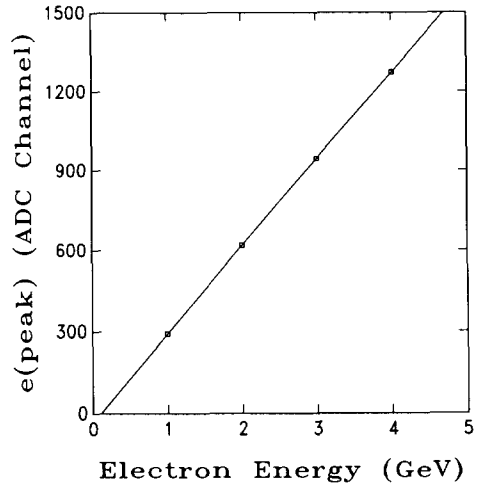


Fig. 9. Energy linearity data for the electron beam at 1 to 4 GeV.

- iv) determine the position resolution of the calorimeter for electromagnetic showers.
- Finally,  $\pi^0$  decays were reconstructed and served as a measure of the overall performance of the calorimeter.

### 5.2. Test setup

The three wedges were supported on a horizontal stand with three degrees of freedom, such that any of the sixty blocks could be aligned with the beam. This is illustrated in fig. 8, which shows the beam hitting block 8 in the middle wedge. The  $X$  direction corresponds to  $\theta$  and the  $Y$  to  $\phi$ .

The beam was tuned to energies of 1, 2, 3, and 4 GeV with a spread of  $\pm 0.8\%$  ( $\sigma(E)/E$ ). The last two quadrupoles could be turned off to get a broad, defocused beam. A threshold cerenkov counter was used to tag electrons (2%) in the beam, which contained  $e^-$ 's,  $\pi^-$ 's,  $K^-$ 's, and  $\bar{p}$ 's. Time-of-flight measurements of  $e^-$ 's and  $\bar{p}$ 's in the beam were used to check the beam energy. Two proportional wire chambers (PWC1,2) with 1 mm pitch were used to track particles. The scintillators S1 and S2 ( $100 \times 150 \text{ mm}^2$  each). S3 ( $10 \times 10 \text{ mm}^2$ ) and S4 ( $100 \times 100 \text{ mm}^2$ ) were used in different combinations to define charge and neutral triggers for the different runs. The signals from the counters were split, 95% being sent to the individual ADCs and 5% to a summer circuit [24].

### 5.3. Results

#### 5.3.1. Energy linearity and resolution

The energy measurement for the electrons hitting the center of a block is shown in fig. 9. The 1, 2, 3, and 4 GeV data represent the peak value for the total energy (summed energy for the hit block and its eight neighbors). The data show a linear response between 1 and 4 GeV, with a slope of (326.4–4.3) ADC channels/GeV and an intercept of  $(-34.6 \pm 2.0)$  ADC channels. The negative intercept is not an artifact of the ADC or the particular counter. The response at low energies is discussed in section 4. The photoelectrons/MeV was determined to be 3.5 for counters with 3 in. and 2.5 in. PMTs, 2.2 for the counters with 2 in. PMTs, and 2.0 for the counters with 1.5 in. PMTs.

Energy resolution for blocks 5, 10 and 15 were found after applying cuts on the direction of the electron beam and restricting the beam to the center of the block. The ratio of the width  $\sigma(E)$  to the peak value  $E$  of the electron total energy distribution is the same, within errors, at each beam energy for the three different blocks. The mean value for  $\sigma(E)/E$  is plotted against  $1/\sqrt{E}$  [GeV] in fig. 10. Taking the average of  $\sigma(E)/E$  for the three blocks and fitting to the form

$$\frac{\sigma(E)}{E} = \frac{A}{\sqrt{E}[\text{GeV}]} + B \quad (1)$$

gives  $A = (2.8 \pm 0.3)\%$  and  $B = (0.3 \pm 0.5)\%$ . Unfolding the measured beam energy spread one obtains  $A = (3.0 \pm 0.3)\%$  and  $B = (-0.04 \pm 0.47)\%$ . The average resolution for electrons uniformly distributed over the face of the middle wedge was found to be  $(3.0 \pm 0.3)\%/\sqrt{E}[\text{GeV}] + (1.5 \pm 0.5)\%$ .

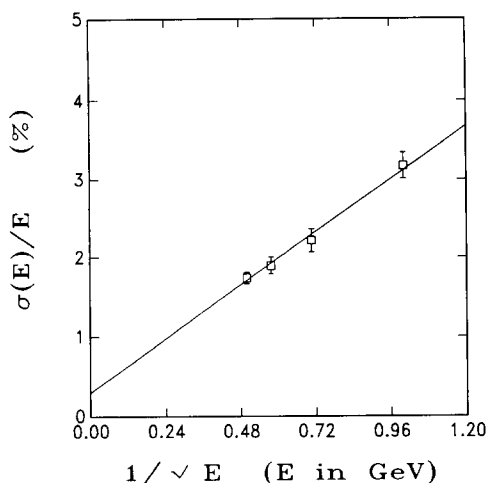


Fig. 10. Energy resolution data fitted to a straight line showing  $1/\sqrt{E}$  [GeV] dependence.

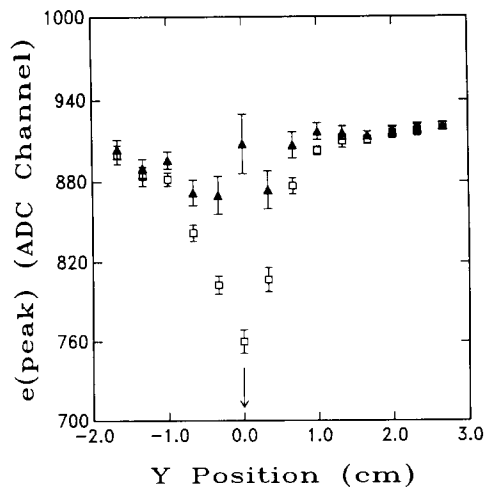


Fig. 11. Total electron energy measured as a function of the position of the electron hit. The open squares indicate uncorrected data and the solid triangles corrected data. The arrow marks the boundary position between the blocks.

#### 5.3.2. Energy sharing and losses

Energy loss in the steel partition between the blocks was found to be less than a few percent in the  $X$  (or  $\theta$ ) direction and 15–20% in the  $Y$  (or  $\phi$ ) direction. This is expected since there is six times more steel between the blocks along the  $Y$  direction than along the  $X$  direction. The open squares in fig. 11 show the peak values of the total electron energy as a function of position along the  $Y$  direction, with the beam position restricted to a region at least 2 cm away from the block edge along the  $X$  direction. The beam energy for these data points was 3 GeV. The center of the dip in the graph is the boundary between two blocks in different wedges. For this pair of blocks the observed maximum energy loss is 20%. The fractional energy loss is parameterized in the form

$$\frac{\Delta E}{E} = A e^{(-y/\lambda)}, \quad (2)$$

where  $y$  is the distance from the block boundary. The parameters  $A$  and  $\lambda$  were fitted for many different pairs of blocks and at different energies. The mean and the spread of the half width parameter  $\lambda$  are 0.42 cm and 0.08 cm, respectively, and depth parameter  $A$ , 16.1% and 2.4%, respectively.

These parameters can be used to correct for energy loss on an event by event basis. The corrected values for the electron energy peaks are shown as solid triangles in fig. 11. The correction has reduced the average energy measurement loss to around 5%, comparable to the average resolution of the detector. The energy resolution for 3 GeV electron hits along  $X$  and  $Y$  are shown in fig. 12a and b, respectively. The energy resolution  $\sigma(E)/E$  deteriorates to 4% in the  $X$  (or  $\theta$ ) boundary

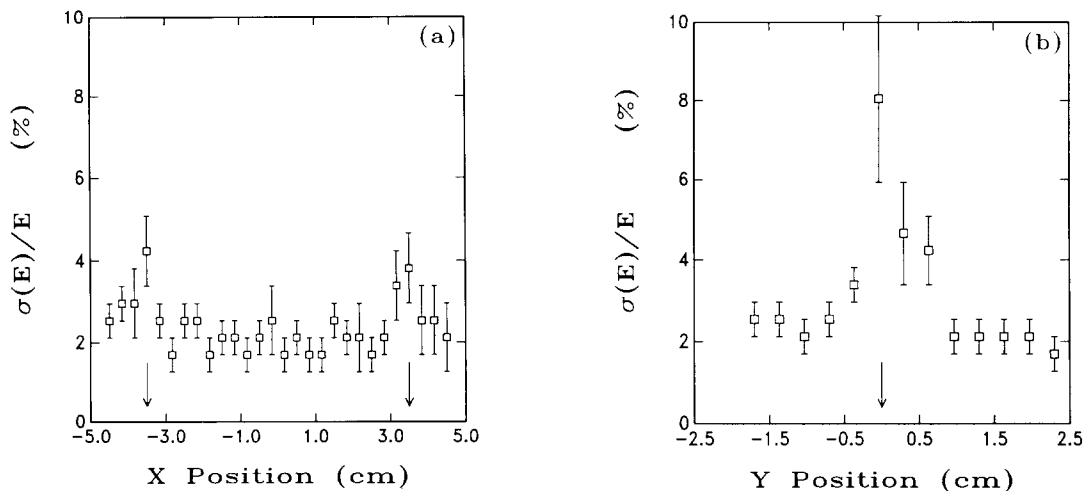


Fig. 12. Energy resolution as a function of position across the face of the blocks, showing (a) resolution for the  $X$  scan and (b) resolution for the  $Y$  scan. The arrows mark the boundaries between the blocks.

regions of the blocks (fig. 12a) and to 8% in the  $Y$  (or  $\phi$ ) boundary region (fig. 12b).

### 5.3.3. Pion-to-electron response ratio

Since calibration with cosmic rays was to be used for the majority of the counters, the energy equivalent of straight-through particles was measured. A straight-through pion was defined by requiring energy deposited only in the hit block. A typical straight-through pion energy distribution is shown in fig. 13 (middle wedge, block 5). The solid line is a Landau fit to the data used to extract the peak position.

The ratios of pion and electron peak values for single block energy distributions are shown in fig. 14 for the counters in the top (solid triangles) and middle (open

squares) wedges. Position and angle cuts were applied to electron data to accept a parallel beam and to restrict the beam to a  $2 \times 2 \text{ cm}^2$  region at the center of the front face of the block. The change in the ratio from blocks 1 to 7 reflects the increase in the block length; the values for block 19 and 20 reflect the smaller transverse size of these counters. The agreement within  $\pm 1.5\%$  (rms) of the two sets of data indicates that this ratio is a constant for blocks of a given shape and shows the uniformity of the manufacturing process and assembly. Therefore the initial energy calibration for the remaining counters could be done using straight-through particles, e.g. cosmic rays.

The straight-through pion to electron response ratio, where the electron response is obtained from the

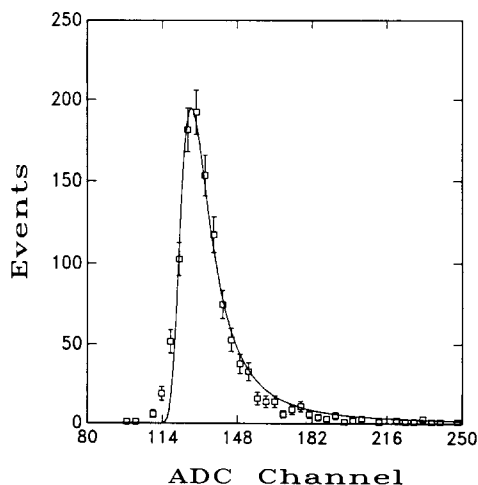


Fig. 13. Pion ADC channel distribution for block 5. The line is a Landau fit to the data points.

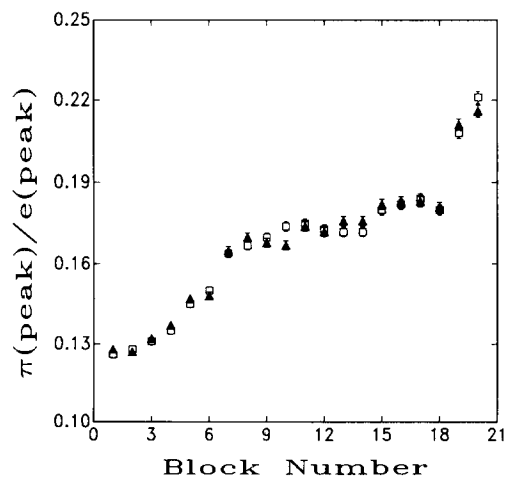


Fig. 14.  $\pi/e$  pulse height ratio for top wedge blocks (solid triangles) and middle wedge blocks (open squares)

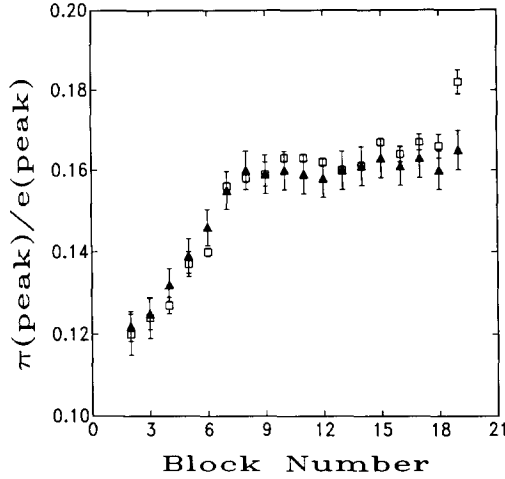


Fig. 15.  $\pi/e$  pulse height ratio summed over nine counters (open squares) and EGS4 Monte Carlo simulation (solid triangles).

summed energy of 9 blocks, is compared in fig. 15 to a Monte Carlo simulation. The electron shower was generated using EGS4 [25] and ray tracing was performed on the cerenkov light produced to obtain the response. For straight-through pions the effects of  $dE/dx$  losses, multiple scattering, and delta rays were included. The end blocks 1 and 20 were not considered. One sees good agreement between the data (open squares) and Monte Carlo results (solid triangles) for all the blocks except 19. A possible factor contributing to this difference is the block size becoming comparable to the size of the shower profile. This leads to a significant amount of energy loss in the steel partition between the blocks which was not taken into account in the simulation.

#### 5.3.4. Position resolution

A method has been developed to find the cluster centroid. It is known that when the centroid is calculated using the energy weighted average of the hit block and its neighbors, the centroid is pulled towards the center of the hit block. This is due to the narrow Gaussian peak of the transverse shower profile around the hit point which leads to a larger energy deposit in the hit block.

In order to correct for this effect, the contribution of the hit block is reduced by a factor  $f$  in calculating the weighted average, if the fraction of energy in the hit block is greater than a specified value  $R$ . Thus we can write

$$X_{\text{Clus.}} = \frac{fE_0x_0 + \sum_{i=1}^8 E_i x_i}{fE_0 + \sum_{i=1}^8 E_i}, \quad (3)$$

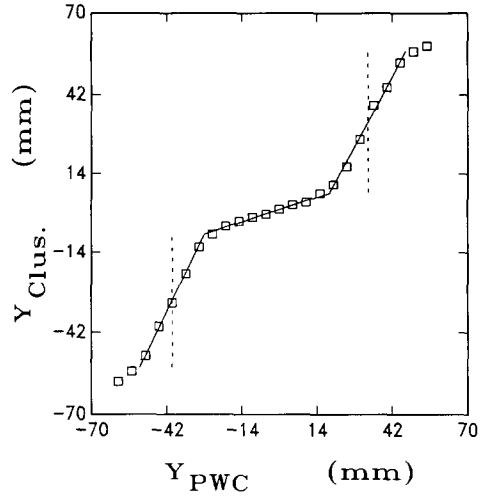


Fig. 16 PWC position versus cluster centroid position where the cluster centroid was calculated using an  $f$  value of 0.4. The dashed lines indicate the boundaries between the blocks.

where  $f = 1.0$  if  $E_0/E_{\text{TOT}} < R$  and  $f < 1.0$  if  $E_0/E_{\text{TOT}} > R$ , and a similar equation for  $Y_{\text{Clus.}}$  follows. By comparing the position as predicted by the PWCs and as obtained from eq. (3), an optimum value of  $f = 0.4$  was found with  $R$  set to 60%. This gave a 25–30% improvement in the overall resolution (from 19 mm for  $f$  always set to 1 to 13.5 mm).

Using these values of  $f$  and  $R$  the cluster centroids ( $X_{\text{Clus.}}, Y_{\text{Clus.}}$ ) were calculated and compared with hit positions ( $X_{\text{PWC}}, Y_{\text{PWC}}$ ). A plot of  $Y_{\text{PWC}}$  versus  $Y_{\text{Clus.}}$  is shown in fig. 16, indicating the ‘‘S’’ curve noted frequently in the literature [26]. An approximate represen-

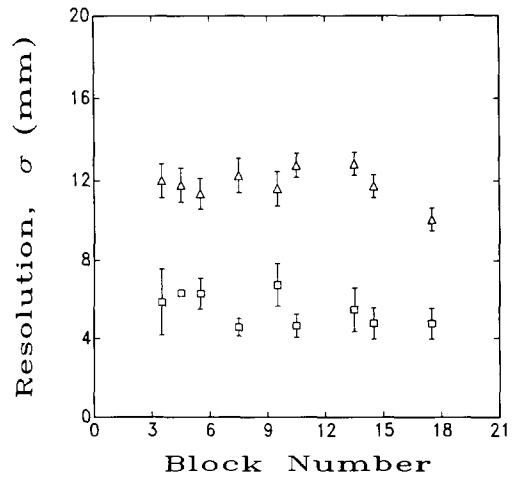


Fig. 17. Position resolution obtained with the clusterization method described in the text. The triangles represent the resolution at the center of the blocks and the squares the boundary region.

tation of the data can be made with three straight line segments as shown. The slope is small in the center region where the position sensitivity is least. The position sensitivity is best near the boundaries.

The parameters of the line fits were used to obtain “corrected” positions from the calculated cluster centroid ( $f=0.4$ ). Position resolutions obtained with the “corrected” cluster centroid for different blocks are shown in fig. 17. The triangles represent resolutions in the center region of the block and the squares represent resolutions near the boundaries. PWC resolution and multiple scattering have been unfolded from the resolution values near the boundary. The resolution in the center of the block improves as the transverse size of the block becomes smaller. The average position resolution of the calorimeter is 9 mm.

### 5.3.5. $\pi^0$ -zero data

Neutral trigger data were recorded using an aluminum target ( $43 \times 34 \times 6.35 \text{ mm}^3$ ) indicated in fig. 8. The S4 counter was placed just downstream of the target and used as a veto in coincidence with S1, S2 and S3 and the “summer” to define a neutral trigger. The wedges were oriented so that block 8 of the middle wedge was along the beam line. Interactions of 3 GeV pions with the target were recorded using the neutral trigger to obtain a sample of  $\pi^0$ 's.

To reconstruct the direction and energy of the two  $\gamma$ 's from  $\pi^0$  decay, the counter with the highest energy was picked as the nucleus of a  $\gamma$ -ray shower. This counter and its eight neighbors were used to define the cluster and to find the cluster centroid. The process was repeated until all clusters were found. Invariant masses were calculated using all combinations of pairs of clusters. The clusters were required to have at least 100 MeV energy each and the centroids to be separated by more than 2 block widths. A  $\pi^0$  peak, found using the energy-weighted average ( $f=1$ ), is shown in fig. 18a. The line is a fit to a  $\pi^0$  Gaussian peak plus a second broad Gaussian background. The  $\pi^0$  exhibits a width of  $(20.1 \pm 0.8) \text{ MeV}/c^2$  at  $(134.7 \pm 0.6) \text{ MeV}/c^2$ . Using the method described in the previous section to obtain “corrected” cluster positions, the width of the  $\pi^0$  peak becomes  $(16.3 \pm 0.6) \text{ MeV}/c^2$  (fig. 18b). Finally, selecting events with the corrected cluster position in the middle wedge for both  $\gamma$ 's in order to minimize energy leakage, one obtains a width of  $(13.9 \pm 1.0) \text{ MeV}/c^2$  with the peak value at

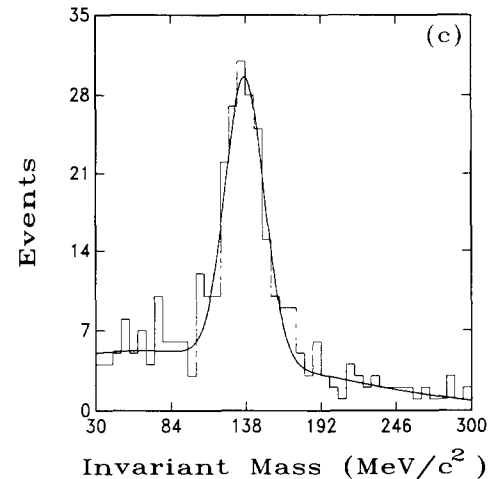
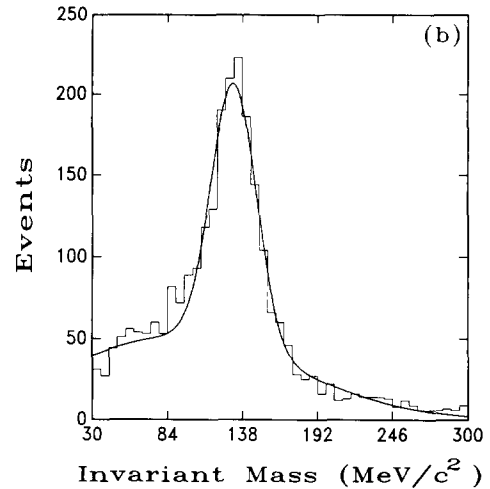
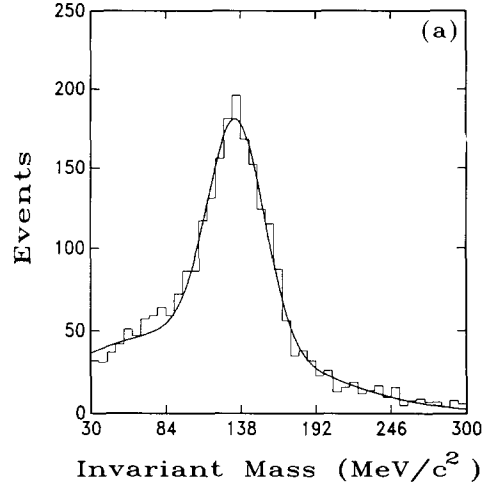


Fig. 18. Gamma-gamma invariant mass distribution from neutral trigger data using (a) simple cluster centroid calculation and (b) the clusterization method described in the text. The distribution with both  $\gamma$ 's restricted to the middle wedge is shown in (c).

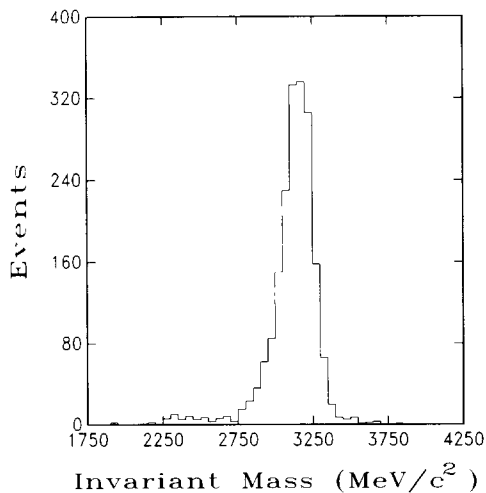


Fig. 19. Invariant mass distribution for  $J/\psi \rightarrow e^+e^-$  trigger data.

$(137.3 \pm 1.1) \text{ MeV}/c^2$  (fig. 18c). The width of the  $\pi^0$  peak is consistent with the average energy and position resolutions discussed previously.

## 6. Preliminary results from Fermilab

The calorimeter was fully assembled, mated to the other parts of the E760 apparatus and installed in late June 1990. In the early running it has performed according to specification allowing clean identification of charmonium decays. As an example, fig. 19 shows the  $J/\psi \rightarrow e^+e^-$  mass as reconstructed in the calorimeter using preliminary calibration constants and making a simple correction for energy lost in the material between wedges. Events were identified as  $J/\psi$  candidates by requiring signals in the Cherenkov counters, two coplanar hits in the hodoscope H2, and exactly two energy clusters in the calorimeter with a total energy greater than 50% of the beam energy. With these simple cuts, the signal is seen to be very clean.

## 7. Conclusions

The E760 central calorimeter consisting of 1280 lead-glass blocks is operational. Test confirmed the uniformity of lead-glass block fabrication and showed that calibration of a block of one shape can be transferred to other blocks of the same shape. Energy measurements with the calorimeter are linear between 1 and 4 GeV and the response of a counter to 88 MeV electron beam is about 90% of that predicted from higher energy results. The best energy resolution of the calorimeter is  $\sigma(E)/E = 3\%/\sqrt{E [\text{GeV}]}$  and the aver-

age energy resolution is  $(3.0 \pm 0.3)\%/\sqrt{E [\text{GeV}]} + (1.5 \pm 0.5)\%$ .

The steel partitions between blocks in  $\phi$  cause an energy loss of up to 20% and degradation of energy resolution to  $8.0\%/\sqrt{E [\text{GeV}]}$  over a small region. A correction reduces the energy loss to the 5% level, comparable to the average resolution of the detector. The position resolution obtained from a special clusterization algorithm is 4–5 mm near the boundary and 1.0–1.2 cm in the center region of the block, with an average position resolution of 9 mm.

## Acknowledgements

We would like to thank Jeff Western, Joel Misek, Jay Hoffman, and Don Goloskie of Fermilab for their help and support with the design and construction of the calorimeter, John Passaneau of Pennsylvania State University for constructing the stand for the BNL test, and Chuck Chizzo, Eileen Hahn, and Bud Koecher of Fermilab for their work in assembling the calorimeter. We are grateful to the staffs of BNL, and especially the Multi-Particle Spectrometer (MPS) group, and UINPL for permitting use of their beams and help during set up and data acquisition. Finally we appreciate the continuing support of our E760 colleagues.

## References

- [1] R.M. Baltrusaitis et al., Phys. Rev. D35 (1987) 2077 (MARK III Collaboration at SLAC);  
D. Bisello et al., Phys. Lett. B179 (1986) 294 (DM2 Collaboration at DESY);  
J.E. Gaiser et al., Phys. Rev. D34 (1986) 711 (Crystal Ball Collaboration at SLAC).
- [2] E.D. Bloom and C.W. Peck, Ann. Rev. Nucl. Sci. 33 (1983) 143;  
G. Abrams et al., Phys. Rev. Lett. 43 (1979) 477;  
G. Abrams et al., Phys. Rev. Lett. 43 (1979) 481.
- [3] F. Gilman, Charmonium Physics, Proc. CCAST (World Laboratory) Symp./Workshop, eds. Ming-han Ye and Tao Huang (Gordon and Breach, 1988) p. 1.
- [4] C. Baglin et al., Charmonium Spectroscopy at the ISR using an Antiproton Beam and a Hydrogen Gas Jet Target, EP Int. rep. 85-01, CERN (1985).
- [5] J. Peoples Jr., in: Low Energy Antimatter, Proc. Workshop on the Design of a Low Energy Antimatter Facility, Madison, 1985, ed. D. Cline (World Scientific, 1986) p. 144;  
V. Bharadwaj et al., Proc. Europ. Particle Accelerator Conf., Rome, 1988, ed. S. Tazzari (World Scientific, 1989) p. 395;  
V. Bharadwaj et al., Proc. Europ. Particle Accelerator Conf., Rome, 1988, ed. S. Tazzari (World Scientific Publishing Co., 1989) p. 964.  
V. Bharadwaj et al., Operation of the Fermilab Accumula-

- tor for Medium Energy Proton–Antiproton Physics, to appear in Proc. Europ. Particle Accelerator Conf., Nice, France, 1990.
- [6] C. Baglin et al., Phys. Lett. B172 (1986) 455; C. Baglin et al., Phys. Lett. B171 (1986) 135; C. Baglin et al., Phys. Lett. B187 (1987) 191; C. Baglin et al., Nucl. Phys. B286 (1987) 592; C. Baglin et al., Phys. Lett. B195 (1987) 85; C. Baglin et al., Phys. Lett. B225 (1989) 296.
- [7] C. Biino et al., Nucl. Instr. and Meth. A271 (1988) 417; C. Biino et al., IEEE Trans. Nucl. Sci. NS-36 (1989) 98; R. Calabrese et al., IEEE Trans. Nucl. Sci. NS-36 (1988) 54; R. Calabrese et al., Nucl. Instr. and Meth. A277 (1989) 116.
- [8] M.A. Hasan et al., The Fermilab E760 Forward Electromagnetic Calorimeter, Nucl. Instr. and Meth. A295 (1990) 73.
- [9] K. Kırsebom and R. Sollie, Nucl. Instr. and Meth. A245 (1986) 351.
- [10] The blocks were cast by Schott Glass Technologies, Inc., Duryea, PA, USA, and cut to specified size and polished by Cosmo Optics, Inc., Middletown, NY, USA.
- [11] It was found during construction that relaxing the requirement of the surface finish did not affect the light output. The glass block surfaces were pre-polished with 15  $\mu\text{m}$  alumina abrasive, and then felt-polished for 2.5 h with 2.5  $\mu\text{m}$  cerium oxide abrasive, rather than the original process of 9  $\mu\text{m}$  alumina prepolishing followed by 5 h of felt-polishing with 2.5  $\mu\text{m}$  cerium oxide.
- [12] Epoxy Technology Inc., Billerica, MA, USA.
- [13] Two and a half turns of 0.1 mm thick and 10 cm wide Permalloy 80 (80% Ni, 14.89% Fe, 4.34% Mo, 0.47% Mn, and 0.29% Si) manufactured by Spang Speciality Metals, Butler, PA, USA (formerly Magnetics Inc.)
- [14] Laser Machining, Somerset, WI, USA.
- [15] Series M, 20 position HV special applications connector blocks with a diallyl phthalate pin housing manufactured by AMP Inc., Harrisburg, PA, USA. Subminiature Coaxicon contacts and RG-174 coaxial cable for the signal path and type II pins and RG-58 coaxial cable for the HV path were used.
- [16] LeCroy Research Systems, West Nyack, NY, USA, model 4300B, 11-bit option, 500 pc full scale.
- [17] EG and G part number FX-200, EG and G Electro-Optics, Salem, MA, USA.
- [18] Mitsubishi part number EH400, Mitsubishi Rayon America Inc., New York, NY, USA.
- [19] Schott Glass Technologies, Inc., Duryea, PA, USA, Blue filter: BG-37, Green filter: GG-455, Neutral density filter: KG-3.
- [20] Amphenol part numbers 905-119-5052 and 804-107-03.
- [21] Hewlett Packard part numbers HFBR4501 and HFBR4505.
- [22] R.D. Boltan et al., Nucl. Instr. and Meth. 174 (1980) 411.
- [23] This property has been alluded to previously by H.W. Baer et al., Nucl. Instr. and Meth. 180 (1981) 445.
- [24] R. Ray et al., A Trigger for the Fermilab E760 Lead-glass Calorimeter, to be submitted for publication in Nucl. Instr. and Meth. A.
- [25] R.L. Ford and W.R. Nelson, SLAC rep. 210 (1978); W.R. Nelson et al., SLAC rep. 265 (1985).
- [26] H. Albrecht et al., Nucl. Instr. and Meth. A275 (1989) 1; U. Buchner et al., Nucl. Instr. and Meth. A272 (1988) 695; G.A. Akopdjanov et al., Nucl. Instr. and Meth. 140 (1977) 441.